An INS-Centric Locator for Autonomous Vehicles Aided by GNSS, Monocular Visual-Inertial Odometry, and HD Vector Maps

Chin-Chia Hsu [1], Chi-Hsin Huang [2], Syun Tsai [3], Yi-Feng Chang [4], Kai-Wei Chiang [5], Meng-Lun Tsai [6]

[1] Dept. of Geomatics, National Cheng Kung University, Tainan, Taiwan - chinchia120@geomatics.ncku.edu.tw
[2] Dept. of Geomatics, National Cheng Kung University, Tainan, Taiwan - windstorm@geomatics.ncku.edu.tw
[3] Dept. of Geomatics, National Cheng Kung University, Tainan, Taiwan - dino920135@geomatics.ncku.edu.tw
[4] Dept. of Geomatics, National Cheng Kung University, Tainan, Taiwan - f64066185@gs.ncku.edu.tw
[5] Dept. of Geomatics, National Cheng Kung University, Tainan, Taiwan - kwchiang@geomatics.ncku.edu.tw
[6] Dept. of Geomatics, National Cheng Kung University, Tainan, Taiwan - taurusbryant@geomatics.ncku.edu.tw

Keywords: INS-centric localization, GNSS/INS integration, visual-inertial odometry, extended Kalman filter, HD Vector Maps, autonomous vehicles.

Abstract

Reliable lane-level localization remains difficult for autonomous vehicles (AVs) when Global Navigation Satellite System (GNSS) observations are degraded by blockage, multipath, and non-line-of-sight reception in urban environments. This paper presents PointLoc, an Inertial Navigation System (INS)-centric locator aided by GNSS, monocular visual-inertial odometry (VIO), and High-Definition (HD) Vector Maps. The proposed method is formulated as an INS-centric error-state extended Kalman filter (EKF), in which the INS provides persistent state propagation, while GNSS, VIO, and map matching are incorporated as aiding updates according to their availability and reliability. This design preserves a unified position, velocity, and attitude solution and enables graceful degradation when some aiding sources become unavailable. The method is validated through real-vehicle experiments in Taichung Shuinan and Tainan Shalun under mixed GNSS conditions. The results show that PointLoc achieves the best overall full-route performance in Taichung Shuinan and remains broadly comparable to GNSS/INS/VIO, while still outperforming GNSS/INS, in Tainan Shalun. In the mapped GNSS-denied segment of Taichung Shuinan, PointLoc effectively suppresses vertical drift and substantially improves three-dimensional positioning. The mapped-road analysis further shows that the INS-centric design avoids the planar instability observed in a vision-centric benchmark and provides a more continuous localization solution.

1. Introduction

AVs require reliable lane-level localization because position errors directly affect lane keeping, path planning, and vehicle control. As the level of driving automation increases, localization must support lane-level driving tasks rather than only coarse road-level navigation. The SAE J3016 taxonomy formalizes this progression and clarifies how responsibility shifts from the human driver to the driving automation system. In this context, “Where in Lane” localization is a practical target because it requires the vehicle position to remain accurate enough for consistent lane-level operation, as illustrated in Figure 1 (Stephenson et al., 2011). This requirement becomes difficult to maintain in urban roads, where GNSS quality can change rapidly along the route (Meng et al., 2018).

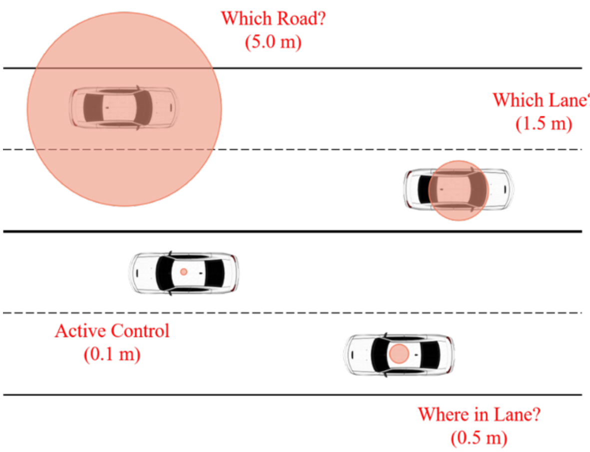

Figure 1. Navigation accuracy classification of AVs.

Conventional integration of the GNSS and the INS remains a fundamental solution for land vehicle navigation because it provides global positioning together with continuous inertial state propagation. Under favourable conditions, GNSS/INS can maintain stable navigation performance. However, in practical road environments, GNSS measurements are often degraded by multipath, NLOS reception, and signal blockage caused by buildings, roadside vegetation, and elevated structures. Once GNSS quality becomes poor or unavailable, the INS can still maintain short-term continuity, but its accumulated errors can no longer be effectively bounded. This limitation makes it difficult for conventional GNSS/INS alone to maintain reliable lane-level localization in mixed driving environments.

To overcome this limitation, many studies have introduced additional sensing sources, especially cameras, to improve localization performance. Vision-based methods can achieve accurate results when image quality is good and visual features remain stable, which makes them attractive for vehicle localization (Leutenegger et al., 2015). However, their performance depends strongly on scene texture, illumination, weather, and occlusion, and once visual tracking becomes weak or fails, the localization result can degrade sharply. In contrast, the INS is self-contained, operates at high frequency, and remains available even when external observations degrade, although it suffers from drift without correction (Matos et al., 2024). This difference motivates the design adopted in this work. Instead of using inertial measurements mainly to support a vision-based estimator, this study treats the INS as the persistent navigation backbone and uses visual information to aid inertial navigation. From a system perspective, this view is also consistent with the modular structure of autonomous driving stacks, in which localization serves as a dedicated subsystem linking sensing and

https://doi.org/10.5194/isprs-archives-XLIX-B1-2026-361-2026 | © Author(s) 2026. CC BY 4.0 License.

map information to downstream planning and control modules, as illustrated in Figure 2 (Autoware Foundation, n.d.).

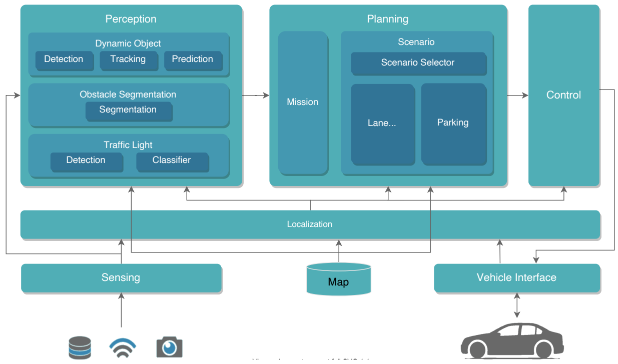

Figure 2. High-level architecture design in Autoware.

To address these requirements, this paper presents PointLoc, an INS-centric locator for AVs aided by GNSS, monocular VIO, and HD Vector Maps. PointLoc is formulated as an INS-centric error-state extended Kalman filter (EKF), in which the INS provides the core state prediction while GNSS, VIO, and HD Vector Maps matching are incorporated as aiding modules according to their availability and reliability. From the perspective of the vehicle stack, PointLoc is designed to function as a single localization module that continuously outputs a unified position, velocity, and attitude solution rather than a set of separate sensor-specific estimates. Through this design, PointLoc can maintain localization continuity under changing sensing conditions and degrade to reduced sensor configurations when some aiding sources become unavailable. The proposed method is validated on real vehicle tests in Taichung Shuinan and Tainan Shalun, which include open sky, GNSS challenging, and GNSS denied segments with partial Lanelet2 coverage.

2. Related Work

2.1 GNSS/INS Integration

The integration of the GNSS and INS remains a fundamental architecture for land vehicle navigation because the two systems provide complementary characteristics. GNSS offers globally referenced positioning, whereas the INS provides high-frequency and continuous state propagation. In practice, two main strategies are commonly adopted, namely loosely coupled (LC) and tightly coupled (TC) integration (Farrell, 2008; Titterton and Weston, 2004). LC integration is widely used because it directly fuses the navigation outputs of the two systems and is relatively simple to implement. TC integration, in contrast, incorporates raw GNSS observations such as pseudorange and pseudorange rate, and can therefore maintain better robustness when the number or quality of visible satellites becomes insufficient for a standalone GNSS solution (Groves, 2013; Shin, 2005).

In LC integration, the measurement update is commonly formed from the discrepancy between the GNSS and INS navigation solutions. A simplified form can be written as

$$\boldsymbol{z}_{LC}^{k} = \begin{bmatrix} \boldsymbol{r}_{INS}^{k} - \boldsymbol{r}_{GNSS}^{k} \\ \boldsymbol{v}_{INS}^{k} - \boldsymbol{v}_{GNSS}^{k} \end{bmatrix} \quad (1)$$

where $\boldsymbol{z}_{LC}^{k}$ = LC measurement vector at epoch k
$\boldsymbol{r}_{INS}^{k}, \boldsymbol{r}_{GNSS}^{k}$ = position estimated from INS and GNSS
$\boldsymbol{v}_{INS}^{k}, \boldsymbol{v}_{GNSS}^{k}$ = velocity estimated from INS and GNSS

This structure is effective when GNSS measurements remain reliable. However, LC integration depends on the availability of a valid GNSS navigation solution, and its performance degrades when GNSS observations are affected by multipath, NLOS reception, or signal blockage. Under prolonged GNSS challenging or GNSS denied conditions, the accumulated INS drift can no longer be sufficiently bounded, which limits the ability of conventional GNSS/INS integration to maintain lane-level localization performance in complex urban environments (Noureldin et al., 2013).

2.2 Visual-Inertial Localization

Visual-inertial localization methods, including VIO, have been widely studied as effective ways to improve vehicle motion estimation by jointly using camera observations and inertial measurements. In these methods, the camera provides geometric constraints from tracked visual features, while the IMU supports motion propagation and scale observability (Forster et al., 2015). Representative approaches include filter-based formulations such as the multi-state constraint Kalman filter (MSCKF), as well as optimization-based methods that combine visual reprojection constraints with inertial pre-integration over a sliding window (Forster et al., 2017). These methods have shown strong performance in local motion estimation and have become an important direction in autonomous navigation and robotics.

Despite these advantages, visual-inertial methods remain strongly dependent on image quality and feature tracking stability. Their performance can degrade under weak texture, illumination changes, motion blur, dynamic objects, and partial occlusion, all of which are common in practical road environments. In addition, VIO primarily provides locally consistent relative motion rather than a stable global reference. As a result, visual-inertial localization alone does not naturally fulfil the role of a persistent vehicle localization module under all driving conditions. For autonomous driving, this limitation is important because the failure of a vision-dominant estimator can directly affect localization continuity. This motivates the use of visual-inertial estimation as a complementary source of motion constraints rather than as the only navigation backbone.

2.3 HD Maps-Aided Localization

HD Maps-aided localization has become an important direction for autonomous driving because prior map information can provide geometric and semantic constraints beyond those available from onboard sensing alone. In road environments, HD Maps can encode lane boundaries, centerlines, road topology, and other traffic-related information that supports lane-level localization. By aligning vehicle observations with mapped road structure, map-aided methods can improve localization consistency, especially when GNSS quality is degraded or when inertial drift needs additional constraints (Levinson and Thrun, 2010).

HD Maps can be represented in different forms, including point cloud maps and vector maps. Point cloud maps preserve dense geometric detail and are well suited to matching with geometry-rich observations, especially in LiDAR-based localization pipelines. However, they usually require larger storage, denser data management, and more extensive map maintenance. Vector maps, in contrast, represent the road using structured elements such as lane boundaries, centrelines, and semantic attributes. This representation is more compact and easier to update, and it is well suited to applications where lane structure and road topology play a central role. At the same time, vector maps contain less geometric detail than point cloud maps and therefore depend more strongly on stable feature extraction and reliable map association. These two map forms therefore reflect different design choices rather than a strict superiority of one over the other.

In this study, HD Vector Maps are adopted as the map representation. This choice is consistent with the lane-level localization objective and with the use of Lanelet2 as the map framework for structured road representation (Poggenhans et al., 2018). Related studies have shown that monocular localization can also be performed using HD Vector Maps when visual observations can be associated with lane-level map features. Nevertheless, map-aided localization still depends on map coverage, observation quality, and matching consistency. A standalone map-matching pipeline therefore does not necessarily provide a persistent full navigation state by itself, even when it can produce lane-consistent position estimates (Xiao et al., 2020).

3. Methodology

3.1 System Overview of PointLoc

PointLoc is designed as an INS-centric locator for autonomous vehicles. Rather than operating as an independent fusion block for a specific sensing modality, it is intended to function as a single localization module for the vehicle stack. Its role is to continuously provide a unified position, velocity, and attitude (PVA) solution under changing sensing conditions. This design choice follows the observation that the inertial navigation system remains available even when external observations become degraded, while other sensing sources are used to constrain inertial drift whenever reliable measurements are available.

The overall architecture of PointLoc is illustrated in Figure 3. The IMU first supports initial alignment and then drives the INS mechanization, which serves as the core state propagation backbone of the system. GNSS provides position aiding to the EKF and supports initialization. In parallel, the monocular camera and IMU are used to form the VIO branch, whose output is screened by odometry fault detection and exclusion (FDE) before being used as velocity aiding. The camera and HD Vector Maps are further processed through the map-matching branch, where image and map information are associated through a particle-filter-based framework. After particle FDE, the resulting position and heading information is supplied to the EKF as additional aiding measurements. The filter integrates these heterogeneous observations with the inertial prediction and outputs the final PVA solution. The estimated error terms, including inertial sensor bias and scale-factor corrections, are then fed back to the INS mechanization to improve subsequent state propagation.

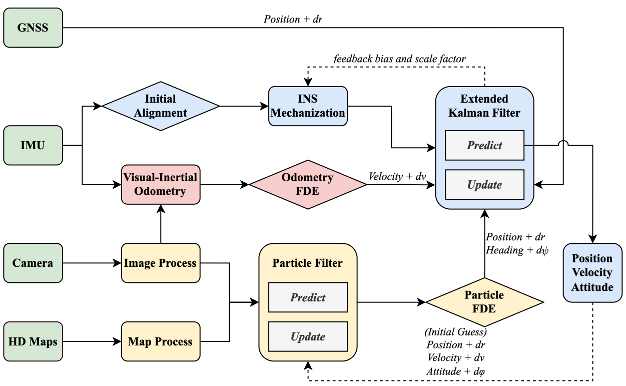

Figure 3. System overview of PointLoc architecture.

Through this architecture, PointLoc maintains a single INS-centric navigation state while allowing different sensing sources to contribute according to their availability and reliability. When GNSS, VIO, and HD Vector Maps matching are all available, the system operates with full aiding. When HD Vector Maps are unavailable, the system degrades to GNSS/INS with VIO aiding. When VIO is also unavailable or rejected, the system can continue operating with GNSS/INS alone. This modular design allows PointLoc to preserve a continuous localization output without changing its external interface to the vehicle stack, which is consistent with its role as a locator rather than a sensor-specific estimator.

3.2 INS-Centric EKF Integration Scheme

PointLoc adopts an INS-centric error-state EKF as the central estimator for maintaining a persistent navigation state in navigation-frame (n-frame). The nominal attitude, velocity, and position are propagated by INS mechanization driven by the IMU, while the EKF estimates the corresponding navigation errors together with inertial sensor bias and scale-factor errors. This structure follows standard INS error-state filtering practice, in which mechanization provides the nominal trajectory and the EKF estimates the uncertainty and correction terms required to bound inertial drift.

The 21-dimensional error-state vector used in PointLoc is defined as

$$\delta\hat{\boldsymbol{x}} = [\delta\boldsymbol{r}^n \quad \delta\boldsymbol{v}^n \quad \delta\boldsymbol{\psi}^n \quad \delta\boldsymbol{b}_g \quad \delta\boldsymbol{b}_a \quad \delta\boldsymbol{s}_g \quad \delta\boldsymbol{s}_a]^T \tag{2}$$

where $\delta\boldsymbol{r}^n$ = position error in n-frame
$\delta\boldsymbol{v}^n$ = velocity error in n-frame
$\delta\boldsymbol{\psi}^n$ = attitude error in n-frame
$\delta\boldsymbol{b}_g$, $\delta\boldsymbol{b}_a$ = bias error of gyro and accelerometer
$\delta\boldsymbol{s}_g$, $\delta\boldsymbol{s}_a$ = scale-factor error of gyro and accelerometer

During the prediction step, the nominal navigation state is propagated by strapdown mechanization, while the error covariance is propagated using the linearized system model and process noise. In discrete form, the error-state propagation can be written as

$$\delta\boldsymbol{x}_{k+1} = \boldsymbol{\Phi}_k\delta\boldsymbol{x}_k + \boldsymbol{w}_k \tag{3}$$

where $\delta\boldsymbol{x}_{k+1}$ = predicted error-state at epoch $k+1$
$\boldsymbol{\Phi}_k$ = state transition matrix
$\boldsymbol{w}_k$ = process noise vector

During the update step, PointLoc incorporates external aiding observations through the same INS-centric EKF framework. GNSS provides globally referenced position observations, the VIO module provides body-frame (b-frame) velocity observations, and the HD Vector Maps matching module provides map-referenced position and heading observations. The innovation is formed between its predicted counterpart from the nominal state and the aiding observation, and the resulting correction is fed back to the nominal navigation solution. A generic measurement innovation can be written as

$$\boldsymbol{z}_k = \hat{\boldsymbol{y}}_k - \boldsymbol{y}_k \tag{4}$$

where $\boldsymbol{z}_k$ = innovation vector at epoch k
$\hat{\boldsymbol{y}}_k$ = predicted observation from nominal state
$\boldsymbol{y}_k$ = aiding observation

In addition to these external aiding sources, the EKF can also incorporate motion constraints derived from the ground-vehicle motion model (Dissanayake et al., 2001). For wheeled vehicle applications, these constraints provide practical information that helps suppress inertial drift when the corresponding motion conditions are satisfied. A zero-velocity update (ZUPT) is applied when the vehicle is stationary, based on the assumption that the true vehicle velocity should be zero. A zero-integrated heading rate (ZIHR) is used to suppress heading drift during stationary intervals by assuming that no true heading change occurs over that period. A non-holonomic constraint (NHC) exploits the fact that a wheeled vehicle normally does not experience significant lateral or vertical slip, so the lateral and vertical velocities in the vehicle frame can be constrained near zero. In PointLoc, these constraints are treated as pseudo-measurements and processed within the same EKF update framework.

3.3 Monocular Visual-Inertial Odometry Aiding Module

The monocular VIO module (Qin et al., 2018) in PointLoc is designed as an aiding source for the INS-centric estimator rather than as an independent localization backbone. By jointly processing monocular camera observations and inertial measurements, the VIO module provides locally consistent motion information that helps constrain inertial drift when GNSS quality becomes poor or unavailable. Unlike GNSS, however, VIO does not provide a globally referenced navigation solution, and its accumulated error may still grow over time. In PointLoc, its role is therefore limited to supplying motion-related observations to the EKF while the INS remains responsible for the persistent state propagation.

Modern VIO methods are commonly implemented through sliding-window optimization, where visual feature constraints and inertial information are combined to estimate short-term motion. In this study, the VIO branch is treated as a local motion estimator that outputs b-frame velocity observations for EKF update. This design is consistent with the INS-centric architecture of PointLoc, because the VIO output is not used to redefine the navigation state itself. Instead, it is used to correct the INS-predicted velocity when the visual solution is considered reliable.

The VIO aiding update is formed from the difference between the INS-estimated b-frame velocity and the VIO-derived b-frame velocity. The velocity innovation can be written as

$$\boldsymbol{z}^{vel} = \boldsymbol{v}_{INS}^{b} - \boldsymbol{v}_{VIO}^{b} = \boldsymbol{R}_{n}^{b}\boldsymbol{v}_{INS}^{n} - \boldsymbol{v}_{VIO}^{b} \tag{5}$$

where $\boldsymbol{z}^{vel}$ = velocity innovation vector
$\boldsymbol{v}_{INS}^{b}$ = INS-estimated velocity in b-frame
$\boldsymbol{v}_{INS}^{n}$ = INS-estimated velocity in n-frame
$\boldsymbol{v}_{VIO}^{b}$ = VIO-derived velocity in b-frame
$\boldsymbol{R}_{n}^{b}$ = rotation matrix from n-frame to b-frame

The effectiveness of this aiding module depends on the quality of visual observations and feature tracking. In practical road environments, the VIO solution can degrade under weak texture, illumination changes, motion blur, dynamic occlusion, or unstable tracking. For this reason, the VIO output is not accepted unconditionally in PointLoc. Instead, it is screened before update, and unreliable odometry observations are rejected. This treatment preserves the INS-centric state definition of the estimator and allows PointLoc to continue operating with the remaining aiding sources when visual conditions are unfavourable.

3.4 HD Vector Maps Matching Aiding Module

The HD Vector Maps matching module in PointLoc provides lane-consistent position and heading constraints when the vehicle operates within mapped road segments. In this module, camera-derived road evidence is associated with the lane-level structure represented by the HD Vector Maps in Lanelet2 format. Unlike GNSS, which provides globally referenced positioning, this branch constrains the navigation state through prior road geometry and topology. In PointLoc, the map branch is treated as an aiding source to the INS-centric estimator rather than as an independent localization backbone.

A particle-filter-based framework (TIER IV, n.d.) is adopted because the map-matching posterior can become multimodal in practical road environments, as illustrated in Figure 4. This is common near intersections, in multi-lane regions, under weak lane markings, or when visual observations are partially degraded. Under such conditions, multiple pose candidates may remain consistent with the observed road structure, and a single Gaussian representation is often insufficient to preserve these competing hypotheses. By maintaining a set of weighted particles, the map-matching module can represent this ambiguity more effectively and can continue refining the pose estimate as more observations become available (Arulampalam et al., 2002).

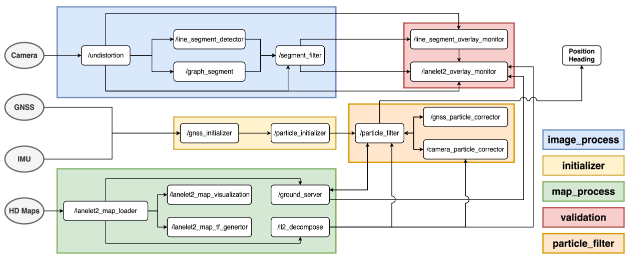

Figure 4. HD Vector Maps matching flowchart.

After prediction, weighting, and resampling, the particle posterior is summarized as a map-referenced position and heading observation with associated uncertainty. The weighted particle mean is used to form the observation, while the particle dispersion is used to characterize its reliability. In this way, the map-matching branch provides lane-level constraints to the EKF without redefining the INS-centric state itself.

The map-derived pose is fused into the INS-centric EKF through loosely coupled position and heading innovations. The position innovation is formed between the INS-estimated position and the map-derived position observation, while the heading innovation is defined as the difference between the INS heading and the map-derived heading. These innovations can be written as

$$\boldsymbol{z}^{pos} = \boldsymbol{r}_{INS}^{n} - \boldsymbol{r}_{MAP}^{n} = \boldsymbol{R}_{e}^{n}(\boldsymbol{r}_{INS}^{e} - \boldsymbol{r}_{MAP}^{e}) + \boldsymbol{R}_{b}^{n}\boldsymbol{l}_{bs}^{b} \tag{6}$$

$$z^{\psi} = \psi_{INS} - \psi_{MAP} \tag{7}$$

where $\boldsymbol{z}^{pos}$ = position innovation vector
z^{ψ} = heading innovation vector
$\boldsymbol{r}_{INS}^{n}$ = INS-estimated position in n-frame
$\boldsymbol{r}_{INS}^{e}$ = INS-estimated position in e-frame
$\boldsymbol{r}_{MAP}^{n}$ = MAP-derived position in n-frame
$\boldsymbol{r}_{MAP}^{e}$ = MAP-derived position in e-frame
$\boldsymbol{R}_{e}^{n}$, $\boldsymbol{R}_{b}^{n}$= rotation matrix from e- or b-frame to n-frame
$\boldsymbol{l}_{bs}^{b}$ = lever-arm vector from the body-frame origin to the map-aiding reference point, expressed in the b-frame
ψ_{INS} = INS-estimated heading
ψ_{MAP} = MAP-derived heading

In implementation, both position and heading updates are accepted only when the map-matching output is internally consistent and the particle posterior indicates a reliable alignment. When the matching result becomes unreliable, the corresponding aiding update is withheld. Therefore, the HD Vector Maps branch contributes only when valid map-based constraints are available, while the overall estimator continues to operate using the remaining sensing sources.

4. Experimental Setup and Data Acquisition

4.1 Experimental Setup

The experimental setup consists of three systems, namely a reference system, a testing system, and a benchmark system. Their sensor configurations and software environments are summarized in Table 1, while the hardware arrangement of the reference and testing systems is shown in Figure 5. The reference system is used to generate a high-accuracy trajectory and attitude reference. The testing system is used to evaluate the proposed PointLoc algorithm. The benchmark system is used to provide a comparison against a vision-centric HD Vector Maps localization pipeline. This arrangement separates reference generation, PointLoc estimation, and baseline comparison within a common experimental framework.

The reference system uses a navigation-grade iMAR iNAV-RQH-10018 IMU together with a NovAtel PwrPak7D-E2 GNSS receiver, and its trajectory is post-processed using Inertial Explorer. The testing system uses the same GNSS receiver model in real-time mode, a MEMS-grade Aceinna OpenRTK330LI IMU, a Basler acA1300-75gc monocular camera, and Lanelet2 HD Vector Maps, and its trajectory is computed by PointLoc. The benchmark system uses the same sensing suite and the same map representation as the testing system, but the localization solution is generated by an Autoware-based localization pipeline.

	Reference System	Testing System	Benchmark System
GNSS	NovAtel PwrPak7D-E2	NovAtel PwrPak7D-E2	NovAtel PwrPak7D-E2
IMU	iMAR-iNAV-RQH-10018	Aceinna OpenRTK330LI	Aceinna OpenRTK330LI
Camera		Basler acA1300-75gc	Basler acA1300-75gc
HD Maps		Lanelet2	Lanelet2
Software	Inertial Explorer	PointLoc	Autoware

Table 1. Summary of systems.

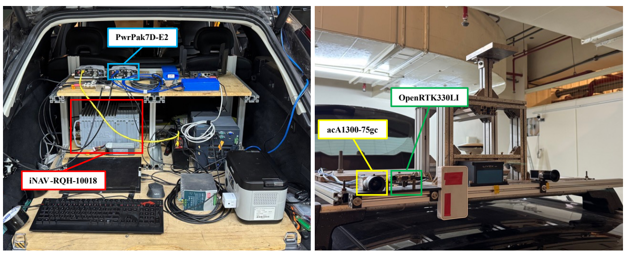

Figure 5. Equipment setup.

The difference between the IMU grades used in the reference and testing systems is summarized in Table 2. The iNAV-RQH-10018 provides substantially better bias stability and noise performance than the OpenRTK330LI. In contrast, the OpenRTK330LI represents a practical MEMS-grade sensing configuration for vehicle localization. This setup therefore allows PointLoc to be evaluated under realistic onboard sensing conditions while still being compared against a higher-grade reference trajectory.

iNAV-RQH-10018	Accelerometer	Gyroscope
Bias Instability	$10\ \mu g$	$0.002\ deg/hr$
Random Walk	$8\ \mu g/\sqrt{Hz}$	$0.0015\ deg/\sqrt{hr}$
OpenRTK330LI	**Accelerometer**	**Gyroscope**
Bias Instability	$20\ \mu g$	$1.5\ deg/hr$
Random Walk	$68\ \mu g/\sqrt{Hz}$	$0.2\ deg/\sqrt{hr}$

Table 2. Specification of IMUs.

4.2 Scenario Description

The real-world testing routes are used in this study, namely Taichung Shuinan and Tainan Shalun. The routes include open sky, GNSS challenging, and GNSS denied segments, together with partial Lanelet2 coverage.

The Taichung Shuinan route has a total length of approximately 5.58 km. As shown in Figure 6, the highlighted segment corresponds to a GNSS denied interval beneath an elevated structure, where satellite visibility is almost completely blocked. The Lanelet2 coverage is shown in the inset of Figure 6 and spans a subset of the route, including the underpass segment. Figure 7 presents the corresponding GNSS PDOP and vehicle velocity profile for this route.

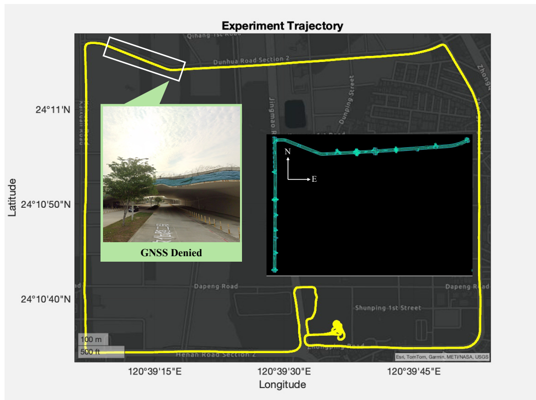

Figure 6. Experiment trajectory and Lanelet2 map in Shuinan.

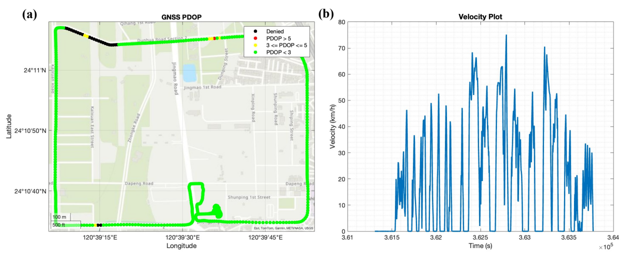

Figure 7. (a) GNSS PDOP; (b) velocity plot in Shuinan.

The Tainan Shalun route has a total length of approximately 6.26 km. As shown in Figure 8, one highlighted segment corresponds to a GNSS denied interval beneath a viaduct, while the other corresponds to a GNSS challenging segment near the Tainan High Speed Rail station. The GNSS challenging segment is outside the Lanelet2 coverage area, so no map-based constraint is available there. Figure 9 presents the corresponding GNSS PDOP and vehicle velocity profile for this route.

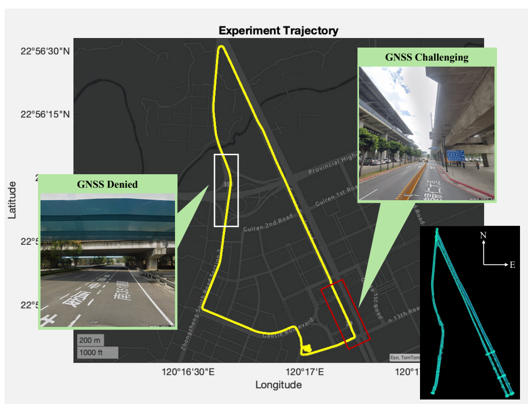

Figure 8. Experiment trajectory and Lanelet2 map in Shalun.

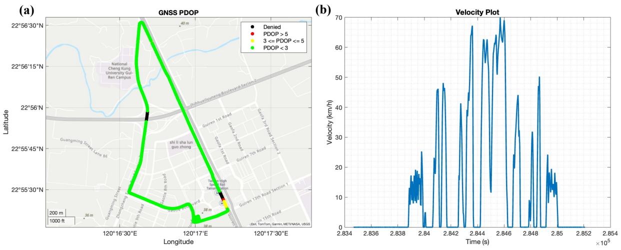

Figure 9. (a) GNSS PDOP; (b) velocity plot in Shalun.

4.3 Accuracy Assessment and Baselines

Localization accuracy is evaluated against a reference trajectory generated from the reference system using navigation-grade GNSS/IMU data and post-processing in Inertial Explorer. The estimated trajectories from GNSS/INS, GNSS/INS/VIO, the benchmark, and PointLoc are synchronized with this reference trajectory before comparison.

The main baselines considered in this study are GNSS/INS, GNSS/INS/VIO, and PointLoc. In addition, a benchmark using the same testing-grade sensing suite and the same Lanelet2 map format is included as a position error baseline. The evaluation is organized into three levels, namely full-route results for Taichung Shuinan and Tainan Shalun, subset-level results under different GNSS conditions, and an additional Lanelet2 coverage subset for mapped-road analysis.

5. Results and Discussion

5.1 Overall Localization Performance

The full-route trajectories in Taichung Shuinan and Tainan Shalun are shown in Figure 10. In the Taichung Shuinan scenario, PointLoc provides the best overall full-route performance among the three configurations. As illustrated in Table 3, the most notable improvement appears in the U and 3D errors, where PointLoc yields a clear reduction in RMSE relative to both GNSS/INS and GNSS/INS/VIO. In addition, the maximum errors are substantially reduced, which indicates that PointLoc not only improves the average route-level accuracy but also suppresses large error excursions over the full trajectory.

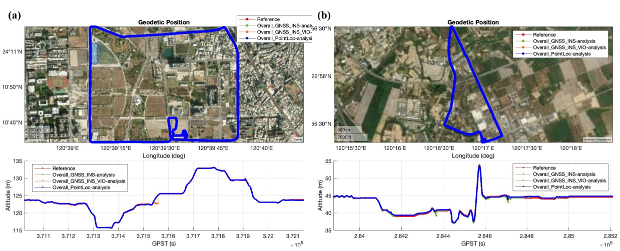

Figure 10. Overall trajectory in (a) Shuinan; (b) Shalun.

Overall Position Error (m) in Taichung Shuinan Scenario					
GNSS/INS	U	2D	3D	Along	Cross
Max Error	-2.471	1.810	2.553	-1.739	-0.562
RMSE	0.222	0.186	0.289	0.162	0.091
GNSS/INS/VIO	U	2D	3D	Along	Cross
Max Error	-2.450	1.561	2.456	-1.532	-0.398
RMSE	0.224	0.151	0.270	0.121	0.090
PointLoc	U	2D	3D	Along	Cross
Max Error	-0.223	0.448	0.453	-0.377	0.343
RMSE	0.062	0.125	0.139	0.086	0.090

Table 3. Overall position error in Shuinan.

In the Tainan Shalun scenario, PointLoc remains clearly better than GNSS/INS at the full-route level, but its overall performance is broadly comparable to GNSS/INS/VIO. The RMSE values in Table 4 show only small differences between these two configurations across the reported position-error metrics, which indicates that the route-level average behaviour is similar when all segments are considered together. This result is also consistent with the fact that the full route contains mixed GNSS conditions and a large open-road portion, so the aggregate statistics do not by themselves reveal the detailed behaviour in the denied and challenging segments.

Overall Position Error (m) in Tainan Shalun Scenario					
GNSS/INS	U	2D	3D	Along	Cross
Max Error	-1.870	1.455	2.369	-1.144	0.899
RMSE	0.287	0.249	0.380	0.207	0.138
GNSS/INS/VIO	U	2D	3D	Along	Cross
Max Error	-1.062	0.595	1.162	-0.583	0.476
RMSE	0.233	0.231	0.328	0.199	0.118
PointLoc	U	2D	3D	Along	Cross
Max Error	-1.125	0.668	1.218	0.655	0.471
RMSE	0.241	0.232	0.335	0.200	0.118

Table 4. Overall position error in Shalun.

5.2 Taichung Shuinan Results

The Taichung Shuinan analysis focuses on the highlighted GNSS denied segment beneath the elevated structure. This behaviour is consistent with the error plot in Figure 11(b). After GNSS outage, both GNSS/INS and GNSS/INS/VIO show a continuous downward trend in the U channel, indicating that VIO alone does not provide an effective constraint against the vertical drift accumulated by inertial propagation in this segment. In contrast, the U error of PointLoc remains close to zero across the denied interval, which indicates that the map-aided update effectively stabilizes the solution against the mapped road surface. The east and north errors are also better bounded, but their improvement is secondary compared with the strong reduction in vertical drift. The trajectory comparison in Figure 11(a) reflects the same pattern. PointLoc remains close to the reference path throughout the denied segment, whereas GNSS/INS and GNSS/INS/VIO exhibit larger deviations after entering the underpass. Overall, the Taichung Shuinan denied-segment result shows that the key contribution of PointLoc in this mapped underpass interval is the suppression of vertical drift after GNSS outage.

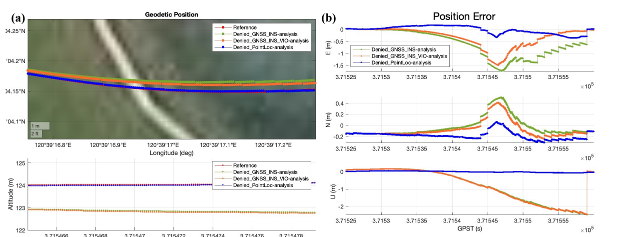

Figure 11. GNSS denied (a) trajectory; (b) error plot in Shuinan.

As shown in Table 5, in this segment, the main advantage of PointLoc is not merely lower position error statistics, but its ability to suppress the vertical drift that dominates the two reduced configurations. Because this underpass interval lies within the Lanelet2 coverage area, PointLoc can continue constraining the INS state through HD Vector Maps matching after GNSS becomes unavailable. This additional map-based aiding provides a stable road-consistent reference that is not available in GNSS/INS or GNSS/INS/VIO, and its effect appears most clearly in the vertical channel.

GNSS Denied Position Error (m) in Taichung Shuinan Scenario					
GNSS/INS	**U**	**2D**	**3D**	**Along**	**Cross**
Max Error	-2.471	1.810	2.553	-1.739	-0.562
RMSE	1.201	0.816	1.452	0.795	0.182
GNSS/INS/VIO	**U**	**2D**	**3D**	**Along**	**Cross**
Max Error	-2.450	1.561	2.456	-1.532	-0.398
RMSE	1.214	0.545	1.331	0.517	0.171
PointLoc	**U**	**2D**	**3D**	**Along**	**Cross**
Max Error	-0.067	0.448	0.453	-0.377	0.302
RMSE	0.039	0.255	0.258	0.191	0.169

Table 5. GNSS denied position error in Shuinan.

5.3 Tainan Shalun Results

The Tainan Shalun analysis includes two degraded segments with different characteristics, namely a GNSS challenging segment and a GNSS denied segment. In the GNSS challenging segment shown in Figure 12, PointLoc remains nearly identical to GNSS/INS/VIO, and both are clearly better than GNSS/INS. This behaviour is consistent with the route condition, because the challenging segment lies outside the Lanelet2 coverage area and therefore no map-based update is available. In this case, PointLoc naturally operates with GNSS/INS and VIO aiding only. The result highlights an important advantage of the INS-centric architecture. When one aiding source is unavailable, the system simply loses one update source rather than losing its primary navigation output. As a result, PointLoc does not collapse in the absence of map aiding and continues to provide stable performance through the remaining VIO velocity updates. The position-error statistics are shown in Table 6.

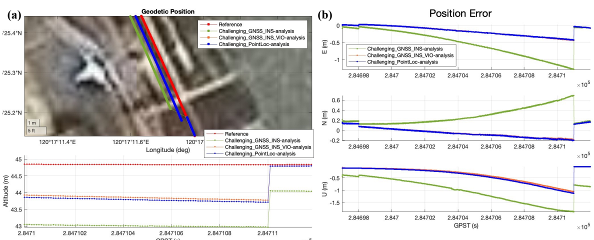

Figure 12. GNSS challenging (a) trajectory; (b) error plot in Shalun.

GNSS Challenging Position Error (m) in Tainan Shalun Scenario					
GNSS/INS	**U**	**2D**	**3D**	**Along**	**Cross**
Max Error	-1.870	1.455	2.369	-1.144	0.899
RMSE	1.124	0.703	1.325	0.558	0.428
GNSS/INS/VIO	**U**	**2D**	**3D**	**Along**	**Cross**
Max Error	-1.062	0.476	1.162	-0.184	0.476
RMSE	0.464	0.233	0.520	0.054	0.227
PointLoc	**U**	**2D**	**3D**	**Along**	**Cross**
Max Error	-1.125	0.471	1.218	-0.184	0.471
RMSE	0.505	0.234	0.556	0.053	0.228

Table 6. GNSS challenging position error in Shalun.

The GNSS denied segment in Figure 13 presents a different situation. In this interval, the visual condition is much darker, so the horizontal contribution of map matching is limited. However, the available map information still provides a constraint in the vertical channel. GNSS/INS exhibits a pronounced altitude drift after GNSS outage, whereas the U error of PointLoc remains much more stable. The denied segment statistics in Table 7 are consistent with this behaviour. Although the horizontal metrics remain broadly comparable to GNSS/INS/VIO, PointLoc achieves the best U RMSE in this segment, which indicates that the map-aided update still helps suppress altitude drift even when its planar correction capability is weak.

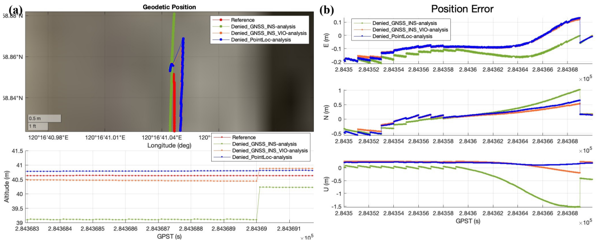

Figure 13. GNSS denied (a) trajectory; (b) error plot in Shalun.

GNSS Denied Position Error (m) in Tainan Shalun Scenario					
GNSS/INS	**U**	**2D**	**3D**	**Along**	**Cross**
Max Error	-1.537	1.026	1.843	1.026	-0.209
RMSE	0.679	0.442	0.810	0.420	0.137
GNSS/INS/VIO	**U**	**2D**	**3D**	**Along**	**Cross**
Max Error	0.262	0.595	0.648	-0.583	-0.127
RMSE	0.215	0.292	0.363	0.276	0.096
PointLoc	**U**	**2D**	**3D**	**Along**	**Cross**
Max Error	0.234	0.668	0.688	0.655	0.135
RMSE	0.192	0.339	0.390	0.325	0.098

Table 7. GNSS denied position error in Shalun.

5.4 Lanelet2 Coverage Results

The Lanelet2 coverage subset is analysed separately because it is the only part of the route where PointLoc and the benchmark can both use map information. In this subset, the comparison is no longer dominated by map availability itself, but by how the localization architecture uses the available map constraints. Figure 14 shows this difference qualitatively. On the straight segment, the benchmark can remain close to the reference when the observed lane geometry is simple, and the association is relatively unambiguous. On the turning segment, however, the benchmark exhibits a much larger planar deviation, which indicates that a vision-centric map-matching output is more sensitive to geometric ambiguity and local observation quality.

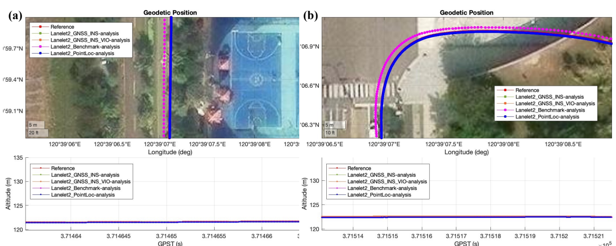

Figure 14. Benchmark in (a) straight; (b) turning road.

A similar pattern appears in Table 8 and Table 9. In both Taichung Shuinan and Tainan Shalun, the benchmark shows much larger planar errors than the INS-centric solutions, even though its U error remains relatively small. This indicates that the main weakness of the benchmark is unstable horizontal map association rather than the absence of map information. Because the benchmark remains constrained near the mapped road surface, its vertical error can appear stable even when the planar alignment is incorrect. By contrast, PointLoc uses HD Vector Maps as aiding constraints within a continuous INS-driven state, which avoids this benchmark-like planar divergence. This advantage is more evident in Taichung Shuinan, where PointLoc shows a clearer reduction in planar error, while in Tainan Shalun it remains far more stable than the benchmark in the planar components.

Lanelet2 Coverage Position Error (m) in Taichung Shuinan Scenario					
GNSS/INS	**U**	**2D**	**3D**	**Along**	**Cross**
Max Error	-2.471	1.810	2.553	-1.739	-0.562
RMSE	0.384	0.281	0.476	0.259	0.108
PointLoc	**U**	**2D**	**3D**	**Along**	**Cross**
Max Error	-0.125	0.448	0.453	-0.377	0.302
RMSE	0.057	0.138	0.149	0.088	0.106
Benchmark	**U**	**2D**	**3D**	**Along**	**Cross**
Max Error	-0.138	3.372	3.373	2.353	-2.644
RMSE	0.057	1.571	1.572	1.405	0.703

Table 8. Lanelet2 coverage position error in Shuinan.

Lanelet2 Coverage Position Error (m) in Tainan Shalun Scenario					
GNSS/INS	**U**	**2D**	**3D**	**Along**	**Cross**
Max Error	-1.537	1.026	1.843	1.026	-0.217
RMSE	0.356	0.211	0.414	0.174	0.119
PointLoc	**U**	**2D**	**3D**	**Along**	**Cross**
Max Error	-0.574	0.668	0.741	0.655	0.219
RMSE	0.220	0.193	0.292	0.160	0.108
Benchmark	**U**	**2D**	**3D**	**Along**	**Cross**
Max Error	-0.650	3.453	3.460	3.440	-2.068
RMSE	0.218	1.606	1.621	1.456	0.678

Table 9. Lanelet2 coverage position error in Shalun.

6. Conclusions

This paper presented PointLoc, an INS-centric locator for autonomous vehicles aided by GNSS, monocular VIO, and HD Vector Maps. In the proposed architecture, the INS maintains the persistent navigation state, while GNSS, VIO, and map matching are incorporated as aiding updates according to their availability and reliability. This design enables PointLoc to preserve a unified and continuous PVA solution under changing sensing conditions, rather than relying on any single aiding source as the final output. The experimental results showed that PointLoc can suppress GNSS outage drift, maintain stable localization in degraded environments, and degrade naturally to reduced sensor configurations when some aiding sources become unavailable. The mapped-road analysis further showed that using HD Vector Maps as aiding constraints, rather than as the sole output source, helps avoid the planar instability observed in a vision-centric benchmark. Overall, these results support PointLoc as an INS-centric locator that emphasizes continuity, bounded behaviour, and graceful degradation for AV applications.

References

Arulampalam, M.S., Maskell, S., Gordon, N., Clapp, T., 2002. A Tutorial on Particle Filters for Online Nonlinear/Non-Gaussian Bayesian Tracking. IEEE Transactions on Signal Processing 50, 174–188. https://doi.org/10.1109/78.978374

Autoware Foundation, n.d. Autoware architecture overview [WWW Document]. URL https://github.com/autowarefoundation/autoware-documentation/blob/main/docs/design/autoware-architecture-v1/image/autoware-architecture-overview.drawio.svg (accessed 7.10.25).

Dissanayake, G., Sukkarieh, S., Nebot, E., Durrant-Whyte, H., 2001. The Aiding of a Low-Cost Strapdown Inertial Measurement Unit Using Vehicle Model Constraints for Land Vehicle Applications. IEEE Transactions on Robotics and Automation 17, 731–747. https://doi.org/10.1109/70.964672

Farrell, J.A., 2008. Aided Navigation: GPS with High Rate Sensors. McGraw-Hill, New York.

Forster, C., Carlone, L., Dellaert, F., Scaramuzza, D., 2017. On-Manifold Preintegration for Real-Time Visual-Inertial Odometry. IEEE Transactions on Robotics 33, 1–21. https://doi.org/10.1109/TRO.2016.2597321

Forster, C., Carlone, L., Dellaert, F., Scaramuzza, D., 2015. IMU Preintegration on Manifold for Efficient Visual-Inertial Maximum-a-Posteriori Estimation, in: Robotics: Science and Systems. Rome, Italy. https://doi.org/10.15607/RSS.2015.XI.006

Groves, P.D., 2013. Principles of GNSS, Inertial, and Multisensor Integrated Navigation Systems, 2nd ed. Artech House, Boston, MA.

Leutenegger, S., Lynen, S., Bosse, M., Siegwart, R., Furgale, P., 2015. Keyframe-Based Visual-Inertial Odometry Using Nonlinear Optimization. Int. J. Rob. Res. 34, 314–334. https://doi.org/10.1177/0278364914554813

Levinson, J., Thrun, S., 2010. Robust vehicle localization in urban environments using probabilistic maps, in: 2010 IEEE International Conference on Robotics and Automation. Anchorage, AK, USA, pp. 4372–4378. https://doi.org/10.1109/ROBOT.2010.5509700

Matos, F., Bernardino, J., Durães, J., Cunha, J., 2024. A survey on sensor failures in autonomous vehicles: Challenges and solutions. Sensors 24, 5108. https://doi.org/10.3390/s24165108

Meng, X., Roberts, S., Cui, Y., Gao, Y., Chen, Q., Xu, C., He, Q., Sharples, S., Bhatia, P., 2018. Required navigation performance for connected and autonomous vehicles: where are we now and where are we going? Transportation Planning and Technology 41, 104–118. https://doi.org/10.1080/03081060.2018.1402747

Noureldin, A., Karamat, T.B., Georgy, J., 2013. Fundamentals of Inertial Navigation, Satellite-based Positioning and their Integration. Springer, Berlin, Heidelberg. https://doi.org/10.1007/978-3-642-30466-8

Poggenhans, F., Pauls, J.H., Janosovits, J., Orf, S., Naumann, M., Kuhnt, F., Mayr, M., 2018. Lanelet2: A high-definition map framework for the future of automated driving, in: 2018 21st International Conference on Intelligent Transportation Systems. Maui, HI, USA, pp. 1672–1679. https://doi.org/10.1109/ITSC.2018.8569929

Qin, T., Li, P., Shen, S., 2018. VINS-Mono: A robust and versatile monocular visual–inertial state estimator. IEEE Transactions on Robotics 34, 1004–1020. https://doi.org/10.1109/TRO.2018.2853729

Shin, E.-H., 2005. Estimation techniques for low-cost inertial navigation (Ph.D. dissertation). University of Calgary, Calgary, AB, Canada. https://doi.org/10.11575/PRISM/2386

Stephenson, S., Meng, X., Moore, T., Baxendale, A., Edwards, T., 2011. Accuracy requirements and benchmarking position solutions for intelligent transportation location based services, in: Proceedings of the 8th International Symposium on Location-Based Services. Vienna, Austria, pp. 76–91.

TIER IV, n.d. YabLoc architecture [WWW Document]. URL https://github.com/tier4/YabLoc/blob/main/docs/yabloc_architecture.drawio.svg (accessed 7.3.25).

Titterton, D.H., Weston, J.L., 2004. Strapdown Inertial Navigation Technology, 2nd ed. Institution of Engineering and Technology, Stevenage, United Kingdom. https://doi.org/10.1049/PBRA017E

Xiao, Z., Yang, D., Wen, T., Jiang, K., Yan, R., 2020. Monocular Localization with Vector HD Map (MLVHM): A Low-Cost Method for Commercial IVs. Sensors 20, 1870. https://doi.org/10.3390/s20071870